

Assessing the impacts of sea-level rise and precipitation change on the surficial aquifer in the low-lying coastal alluvial plains and barrier islands, east-central Florida (USA)

Han Xiao¹ · Dingbao Wang¹ · Scott C. Hagen² · Stephen C. Medeiros¹ · Carlton R. Hall³

Received: 22 October 2015 / Accepted: 5 June 2016 / Published online: 7 July 2016
© Springer-Verlag Berlin Heidelberg 2016

Abstract A three-dimensional variable-density groundwater flow and salinity transport model is implemented using the SEAWAT code to quantify the spatial variation of water-table depth and salinity of the surficial aquifer in Merritt Island and Cape Canaveral Island in east-central Florida (USA) under steady-state 2010 hydrologic and hydrogeologic conditions. The developed model is referred to as the ‘reference’ model and calibrated against field-measured groundwater levels and a map of land use and land cover. Then, five prediction/projection models are developed based on modification of the boundary conditions of the calibrated ‘reference’ model to quantify climate change impacts under various scenarios of sea-level rise and precipitation change projected to 2050. Model results indicate that west Merritt Island will encounter lowland inundation and saltwater intrusion due to its low elevation and flat topography, while climate change impacts on Cape Canaveral Island and east Merritt Island are not significant. The SEAWAT models developed for this study are useful and effective tools for water resources management, land use planning, and climate-change adaptation decision-making in these and other low-lying coastal alluvial plains and barrier island systems.

Keywords Climate change · Numerical modeling · Saltwater intrusion · Surficial aquifer · USA

Introduction

In coastal aquifers, saline and fresh groundwater are in a dynamic equilibrium, and a landward shift of the equilibrium can cause landward encroachment of saline groundwater, resulting in the occurrence of saltwater intrusion (SWI; Bear 1979). Barlow and Reichard (2010) found that SWI occurs by three main pathways including lateral intrusion from seawater, vertical upward intrusion from the deeper saline groundwater, and vertical downward intrusion from storm- or tidal-driven coastal flooding. SWI has been recognized as a global issue with detrimental effects including land salinization, reduction of available freshwater storage, and closure or forced landward relocation of pumping wells (Werner et al. 2013). The magnitude of SWI is dependent on the variability of hydrologic and hydrogeologic settings, the historical spatial and temporal distribution of salinity, and groundwater withdrawal and drainage (Bear et al. 1999).

A saltwater/freshwater transition zone is formed between inland fresh groundwater and coastal saline groundwater, and a landward migration of the transition zone is an effective indicator of the occurrence of SWI (Bear 1979). Groundwater density and salinity in the transition zone is varied spatially and temporally dependent on the regional hydrologic and hydrogeologic conditions (Freeze and Cherry 1979). Due to the complexity and variability of the variable-density condition, numerical methods are usually used to simulate SWI (Anderson and Woessner 1991). The SEAWAT computer code (Guo and Langevin 2002) has been successfully applied to many case studies. Langevin (2003) simulated the submarine groundwater discharge to Biscayne Bay in southeastern Florida, USA.

✉ Dingbao Wang
Dingbao.Wang@ucf.edu

¹ Department of Civil, Environmental, and Construction Engineering, University of Central Florida, 12800 Pegasus Drive, Orlando, FL 32816-2450, USA

² Department of Civil & Environmental Engineering/Center for Computation & Technology, Louisiana State University, Baton Rouge, LA 70803, USA

³ Ecological Program, Integrated Mission Support Services (IMSS) LLC., IMSS-300, Kennedy Space Center, FL 32899, USA

Qahman and Larabi (2006) examined the present condition of SWI and predicted its future behavior under different pumping schemes in the Gaza aquifer in Palestine. Lin et al. (2009) evaluated the current and prospective extents of SWI in the Alabama Gulf Coast, USA. Sanford and Pope (2010) assessed the historical water level and projected the future behavior of SWI on the Eastern Shore of Virginia, USA. Nakada et al. (2011) focused on the subterranean circulation in a tidal flat by modeling the regional-scale submarine groundwater flow. Other notable case studies of additional interest are described in Cobaner et al. (2012), Dausman et al. (2010), Masterson et al. (2014) and Shoemaker and Edwards (2003).

In recent years, the impacts of climate change such as sea-level rise (SLR) and precipitation change, have caused wide public concern (Oude Essink et al. 2010; Sherif and Singh 1999; Sulzbacher et al. 2012; Tang et al. 2013; Webb and Howard 2011). Werner and Simmons (2009) assessed the effect of SLR on a simplified, conceptual, unconfined aquifer and demonstrated that the saltwater invaded and retreated in correspondence with a lowering and elevating of the inland water table. Interpretations of this study confirmed that inland boundary conditions are of great importance for the ‘self-reversal’ mitigation process. Chang et al. (2011) converted the afore-mentioned conceptual model to a case study in the Pioneer Valley of Australia and concluded that SLR does not have as severe of an adverse effect as expected due to the ‘lifting’ of the entire aquifer because of SLR. Rasmussen et al. (2013) conducted a quantitative study to analyze the combined effects of SLR, precipitation change and drainage canals on an island located in the Western Baltic Sea. Likewise, it was demonstrated that the extent of SWI relied strictly on inland boundary conditions.

The low-lying alluvial plains and barrier islands located in the coastal areas of east-central Florida, USA, are vulnerable to flooding from the rising water table driven by SLR (Bilskie et al. 2014; Passeri et al. 2015) since the water-table depth is usually shallow and can even breach land surface during and after a heavy rainfall. Water quality of the shallow coastal aquifer is also vulnerable to SLR-induced SWI, especially during prolonged drought. Hence, the low-lying coastal alluvial plains and barrier islands are dynamically influenced by climate change, and the negative effects include, but are not limited to, shoreline erosion, wetland inundation and migration, SWI, and alterations of the distribution and productivity of vegetation communities (shifts in species composition possibly from less salt tolerant species to more salt tolerant species).

The rate of SLR is expected to accelerate and the probability of severe weather is also expected to increase due to the effects of El Niño (Nicholls and Cazenave 2010; Parker 1991). In 2050, local SLR projections indicated low, intermediate and high scenarios of 13.2, 31.0 and 58.5 cm, respectively, and local precipitation projections indicated that the estimated rainfall would vary from a 7 % decline to a 17 %

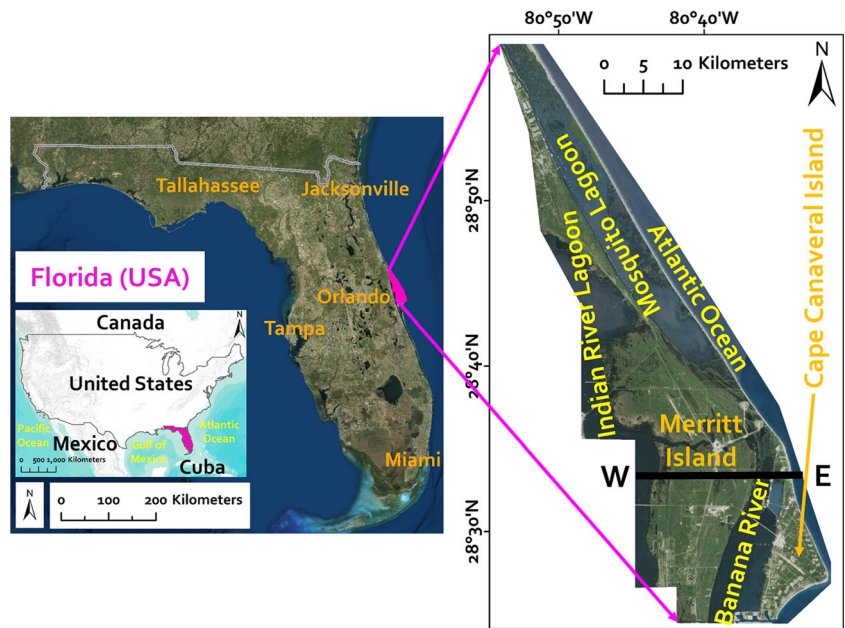
increase compared to 2010 (Rosenzweig et al. 2014). However, the effects of SLR and precipitation change on coastal groundwater flow patterns and salinity distribution are unknown and warrant investigation; therefore, it is of great importance to develop a three-dimensional (3D) variable-density groundwater flow and salt transport model for quantitative assessment.

In inland areas, the surficial aquifer is recharged by direct infiltration of rainfall. Along the coastline, the surficial aquifer contacts the brackish water of the coastal lagoons and seawater of the Atlantic Ocean. The surficial aquifer which has its upper boundary as the water table and lower boundary as the confining unit is extremely important in that it connects the surface-water system to the deeper groundwater system and supports marshes/wetlands, and receives recharge from rainfall and provides discharge to the surrounding coastal lagoons and the Atlantic Ocean; thereby, the surficial aquifer is of primary concern for the effect of SLR and precipitation change. In this study, the SEAWAT code is applied to develop 3D variable-density groundwater flow and salinity transport models for the surficial aquifer of east-central Florida. A reference model is developed and calibrated against field-measured data to simulate the spatial variation of water-table depth and salinity under steady-state 2010 hydrologic and hydrogeologic conditions. The calibrated reference model is then modified to implement five prediction/projection models based on various scenarios of SLR and precipitation change projected to 2050 time frame. The predicted/projected results also contribute to ongoing research that focuses on forecasting vegetation community responses to the projected climate change.

Site description

The study area is Cape Canaveral Barrier Island Complex (CCBIC) located in east-central Florida, which consists of multiple barrier islands, saltwater lagoons, and the Atlantic Ocean coastline. The CCBIC covers an area of approximately 1,000 km² bounded by the Atlantic Ocean to the east, Mosquito Lagoon to the northeast and north, Indian River Lagoon to the west, and Banana River to the southeast and south (Fig. 1). The unique transitional geographic setting between the Caribbean and Carolinian zoogeographic provinces contributes to the area being recognized as having high biodiversity (Hall et al. 2014). The ground-surface elevation varies from −0.2 to 10 m with a regional average of about 1.2 m NAVD 88—LiDAR data from the National Aeronautics and Space Administration (NASA). The variation of topography is relatively small since the region is mainly comprised of broad and flat lowland. Surface water and groundwater flow can be influenced significantly by small changes in land surface elevation because of the flat terrain.

Fig. 1 Location of the Cape Canaveral Barrier Island Complex (CCBIC), Florida (USA)



Hydro-climatologic conditions

According to Mailander (1990), the climate of east-central Florida is humid subtropical with hot/humid summers and mild/dry winters. The wet season is from May to October and the dry season is from November to April. The mean minimum temperatures are 10 °C in January and 22 °C in August, while the mean maximum temperatures are 22 °C in January and 33 °C in July. The amount of annual rainfall varies from 848 to 2,075 mm, with a mean annual rainfall of 1,366 mm.

From Schmalzer et al. (2000), the hydrology of the area is characterized by dynamic interactions between surface water and groundwater, evapotranspiration, and rainfall as shown in Fig. 2 (see the west to east cross-section labeled W–E in Fig. 1). Much of the area is considered micro-tidal (1–2 cm) due to the narrow and distant inlet connections to the Atlantic Ocean. Mosquito Lagoon and Indian River Lagoon are connected by Haulover Canal on the north end of Merritt Island, whereas Indian River Lagoon and Banana River are

connected by a man-made navigation canal, and the canal is connected to the Atlantic Ocean through the Port Canaveral Locks. Water levels in the lagoons are dominated by the annual rise and fall of sea level with a maximum of near 0.0 m (NAVD88) in October. Water flow between the lagoons is primarily driven by wind forcing. In most places, the coastal lagoons have a shallow, flat seagrass-covered bottom with an average depth of 1.5 m. The Intracoastal Waterway is maintained at a depth of 4 m and several basins were dredged to depths of 9–10 m for filling materials during construction of space launch facilities. The total dissolved solids (TDS) concentration in the lagoons typically vary from 10,000 to 45,000 mg/L.

Hydrogeology

From Schmalzer and Hinkle (1990), the hydrostratigraphic units of the CCBIC are composed of, from top to bottom, the surficial aquifer system (SAS), the intermediate confining unit (ICU), the Floridan aquifer system (FAS), and the lower confining unit (LCU). The characteristics of each hydrostratigraphic unit are described in Fig. 3.

As a large and productive aquifer occurring within the Ocala and Avon Park limestone, the general thickness of the FAS is greater than 600 m with mostly very high permeability and transmissivity. In general, the FAS is confined by the silt and clay of the overlying Hawthorn Formation and the underlying Cedar Keys Formation. In most places, the potentiometric level of the FAS is higher than the water table of the SAS, resulting in an upward groundwater seepage from the FAS to SAS, thereby creating a pathway for upward salinity migration. However, the upward seepage is relatively small since

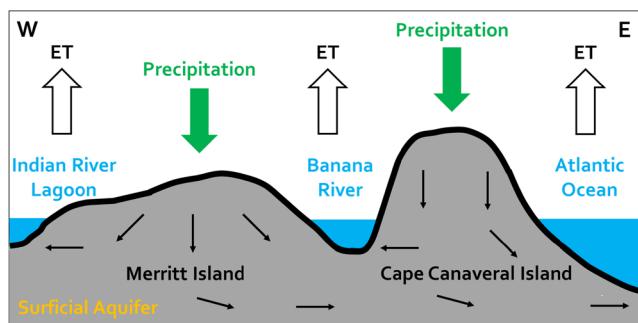


Fig. 2 Illustration of the hydrology of the CCBIC

Table 1 Scenarios of SLR and precipitation change

Year	Case	SLR (cm)	Precipitation
2010	0	0	0
2050	1	13.2	+17 %
	2	13.2	0
	3	31.0	0
	4	58.5	0
	5	58.5	-7 %

the overlying ICU, composed of Hawthorn sediments and Pliocene and upper Miocene deposits, has a very low permeability. The downward seepage through the LCU is extremely small. The highly mineralized water pumped from the FAS is classified as moderately to highly saline water, which greatly limits its consumptive use.

The SAS, which has its upper boundary as the water table and lower boundary as the top of the ICU, occurs in the saturated part of the moderate- to low-permeability Holocene and Pleistocene sediments of fine to medium sand, coquina, silt, shell and marl. The inflow is infiltrated rainwater and upward seepage from the underlying FAS, and the outflow is evapotranspiration and discharge to surface water. The primary recharge areas are located at the relatively higher sand ridges on Cape Canaveral Island and east Merritt Island, and the groundwater flow directions are indicated in Fig. 2. The water table rises to its highest level late in the wet season (September to October) and drops to its lowest level late in the dry season (March to April). The thickness and migration of the saltwater/freshwater transition zone formed in the coastal areas is mainly dependent on the characteristics of the hydrogeologic settings and the fluctuation of the inland water tables. The transition zone can move either landward or seaward in correspondence with lowering or elevating water tables.

Numerical modeling

Model development

A reference model is implemented to simulate the spatial variation of water-table depth and salinity in the SAS under steady-state 2010 hydrologic and hydrogeologic conditions. The reference model is calibrated against the field-measured groundwater levels monitored from 2006 to 2014 and the spatial distribution of marshes/wetlands classified by a land use and land cover map. The calibrated reference model is crucial in this study in that it serves as the ‘foundation’, and the prediction/projection models that incorporate various scenarios of SLR and precipitation change are developed based on it. The reference and prediction/projection models are simply developed for the

SAS due to: (1) the SAS is of primary concern for climate change; (2) the SAS plays a crucial role in the interaction of surface water and groundwater, supporting marshes/wetlands and providing groundwater discharge to the surrounding coastal lagoons and the Atlantic Ocean; (3) salinity of the SAS is extremely important to the biodiversity ecosystem and the survival of the threatened and endangered species of wildlife; (4) the upward salinity migration from the underlying FAS to the SAS is assumed to be negligible due to the relatively small upward groundwater seepage; (5) simulation of groundwater flow and salt transport in the underlying FAS is not important since the FAS is highly mineralized which greatly limits its consumptive use. The advantages of this ‘simple’ model set-up include: (1) the capability to implement finer vertical discretization so that the vertical salinity gradient and the thickness and migration of saltwater/freshwater transition zone can be accurately simulated; (2) less computational demand; (3) reduced simulation assumptions because the hydrogeologic characteristics of the ICU and FAS are unknown due to lack of geophysical survey. The disadvantage of it is a sacrificed accuracy of simulated salinity at the local-scale since the upward SWI from the underlying FAS is not considered.

In view of the calibrated reference model, five prediction/projection models are implemented by modifying the boundary conditions that represent precipitation and water levels of the coastal lagoons and the Atlantic Ocean, to quantify the effects of SLR and precipitation change, based on the assumption that all of the other hydrologic and hydrogeologic conditions remain unchanged from 2010.

Scenarios of SLR and precipitation change

Compared to 2010, precipitation is estimated to vary from 7 % decline to 17 % increase, while SLR scenarios are estimated to be 13.2, 31.0, and 58.5 cm for the low, intermediate, and high ice melt projections, respectively. These downscaled projections for 2050 are developed using data provided by Radley Horton and Daniel Bader, Center for Climate Systems Research, Earth Institute, Columbia University as part of the NASA Climate Adaptation Science Investigators Program (Rosenzweig et al. 2014). Based on these projections, five cases (cases 1–5) are proposed (Table 1).

From a common hydrologic view, increased/decreased recharge to the SAS due to increased/decreased precipitation can alter groundwater salinity. Comparing case 1 to case 2, and comparing case 5 to case 4, it is expected that the extent of SWI of case 1 will be less severe than case 2, and the extent of SWI of case 5 will be more severe than case 4. Comparing case 1 to case 0, however, it is unknown whether the 17 % increase of precipitation can counteract the effect of SLR.

Table 2 Input parameters

Hydrogeologic parameters	Value [units]	Reference
Horizontal hydraulic conductivity (K_h)	15 [m/d]	McGurk and Presley 2002
Anisotropy (K_y/K_z)	10 [-]	
Porosity (n)	0.2 [-]	Blandford et al. 1991
Longitudinal dispersivity (a_L)	6 [m]	Hutchings et al. 2003
Transverse dispersivity (a_T)	0.01 [m]	
Vertical dispersivity (a_V)	0.025 [m]	
Diffusion coefficient (D^*)	0.00128 [m ² /day]	

Simulation code and graphical user interface

The SEAWAT Version 4 (SEAWAT_V4) code developed by Langevin et al. (2008) is selected as the simulation code. Groundwater Vistas, a well-known graphical user interface developed by Environmental Simulations Inc., is used to create model input files.

Spatial and temporal discretization

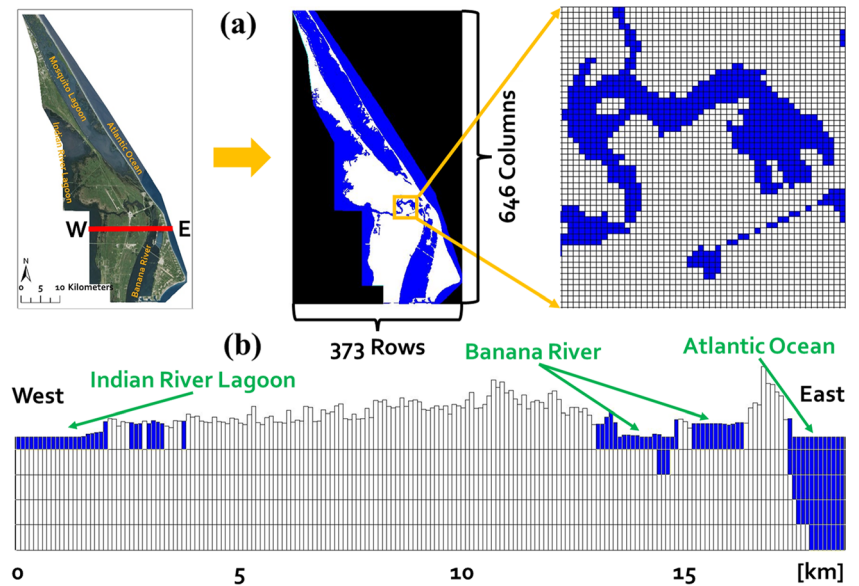
Carefully selecting horizontal and vertical discretization that can effectively represent and identify the saltwater/freshwater transition zone and topographic variations of land surface is essential. The horizontal and vertical discretization is determined by considering enhancing simulation accuracy while maintaining reasonable computer runtimes. In the horizontal plane, the model domain is discretized into 373 rows and 646 columns with a uniform grid spacing of 100 m in both the x-

and y-directions (Fig. 4a). In view of the variable-density condition, a finer vertical discretization in comparison to the constant-density condition is always required for accurate simulation of flow velocities and solute transport (Langevin 2003). Vertically, the model domain is divided into five layers with a uniform layer thickness of 2 m, with the exception of layer 1 (Fig. 4b). The top elevation of layer 1 is set to land surface elevation and 0 m over coastal lagoons and the Atlantic Ocean. The land surface elevation is derived from LiDAR DEM data given by NASA as shown in Fig. 5. The bottom elevation of layer 1 is set at an elevation of -2 m (NAVD 88). The bottom elevation of the SAS is unknown due to lack of stratigraphic data; however, it was estimated by Schmalzer et al. (2000) that the thickness of the SAS is 10–12 m, thereby, the bottom elevation of layer 5 is set to -10 m (NAVD 88). From layer 2 to 5, the layers are flat and have a uniform thickness of 2 m for the purpose of minimizing numerical instabilities. Hence, the model grids in layers 2, 3,

Geologic age	Stratigraphic unit	Hydrostratigraphic unit	Thickness (m)	Lithological character	Water-bearing property
Holocene and Pleistocene	Holocene and Pleistocene deposits	Surficial aquifer system (SAS)	0–33	Fine to medium sand, sandy coquina and sandy shell marl	Low permeability, yields small quantity of water
Pliocene	Pliocene and upper Miocene deposits	Intermediate confining unit (ICU)	6–27	Gray sandy shell marl, green clay, fine sand and silty shell	Very low permeability
Miocene	Hawthorn Formation		3–90	Sandy marl, clay, phosphorite, sandy limestone	General low permeability, yields small quantity of water
Eocene	Ocala Group	Floridan aquifer system (FAS)	0–30	Porous coquina in soft and chalky marine limestone	General very high permeability, yields large quantity of artesian water
			3–15	Soft granular marine limestone	
			>21	Coarse granular limestone	
	>87		Dense chalky limestone and hard, porous, crystalline dolomite		
Avon Park Formation					
Paleocene	Cedar Keys Formation	Lower confining unit (LCU)	–	Interbedded carbonate rocks and evaporites	Very low permeability

Fig. 3 Description of the hydrostratigraphic units

Fig. 4 Spatial discretization: **a** Plan view; **b** West to east cross-section labeled W–E



4, and 5 have a uniform cell volume of $100\text{ m} \times 100\text{ m} \times 2\text{ m}$; however, the volume of each model grid in layer 1 is different because of the topographic variations.

Temporally, the reference and prediction/projection models are steady state, based on the assumption that climate change is gradual and the groundwater systems are in ‘equilibrium’ with climatic factors. This assumption is reasonable in that the purposes of this study are to quantify the long-term climate change impacts rather than the effects of extreme weather (e.g., hurricanes, storm surge). Besides, impacts of human activities are not significant since only a small portion is urbanized and the pumping rate from the 2 extraction wells are very low. Further temporal discretization is introduced in terms of transport time steps for better simulation of salt transport. The length of the transport time step is specified to start with 0.01 day, increasing by a time step multiplier of 1.2, with a maximum transport time step of 100 days. The program does not terminate until steady state is reached.

Hydrogeologic parameters

The specified hydrogeologic parameters are summarized in Table 2. The SAS is assumed to be composed of equivalent porous media, implying that the underground conduits and cavities are not explicitly simulated. This assumption is appropriate and reasonable for implementing a regional-scale numerical model since the complex hydrogeologic conditions in the study area are greatly simplified, despite limiting the interpretation of the model result to the local scale (Langevin 2003; Scanlon et al. 2003).

Boundary conditions

The model domain extends offshore to simulate the interactions between the SAS and coastal lagoons and the Atlantic Ocean with minimal boundary effects. The recharge boundary and the evapotranspiration boundary are assigned to the top of layer 1 to represent the infiltrated rainwater that

Table 3 Results of the second-stage calibration

Situation	‘Simulated’ wetlands	‘True’ wetlands	Percentage of covering area (%)		
			Threshold 0.2 m	Threshold 0.3 m	Threshold 0.4 m
A	Yes	Yes	18.4	21.7	25.0
B	Yes	No	13.7	16.3	18.9
C	No	Yes	21.8	18.4	15.1
D	No	No	46.2	43.6	41.0
Total (%)	–	–	100	100	100
Consistency (%)	–	–	64.6	65.3	66.0

recharges the SAS and the loss of groundwater due to evaporation and plant transpiration. The no-flow boundary is assigned to the bottom of layer 5 since the upward groundwater seepage from the underlying FAS is not simulated. The specified head and concentration boundary and the general head boundary are assigned to represent the lateral boundaries. The well boundary is assigned to represent the two pumping wells.

Specified head and concentration boundary

The specified head and concentration boundary is assigned to the model grids that represent the coastal lagoons and the Atlantic Ocean. In most places, the coastal lagoons are only in layer 1 because of the shallow depth. However, the Atlantic Ocean is obviously much deeper lying in one or more layers, depending on depth to seabed. Due to lack of monitored data, it is assumed that the water levels and TDS concentrations of the coastal lagoons and the Atlantic Ocean are the same. For the reference model, water levels and TDS concentrations are specified to 0 m (NAVD 88) and 35 kg/m³, respectively (Sharqawy et al. 2010). The horizontal view of the specified

head and concentration boundary assigned to layer 1 is visualized in Fig. 6a.

For the prediction/projection models, water levels of the coastal lagoons and the Atlantic Ocean are specified corresponding to SLR scenarios based on the assumption that water levels of the coastal lagoons rise simultaneously at the same magnitude as with the SLR, and TDS concentrations are specified to 35 kg/m³. Further inland encroachment of the coastline is inevitable due to SLR. The new coastline is estimated by comparing the land surface elevation with the ‘new’ sea level, and the coastal lowland that has a lower elevation than the ‘new’ sea level is considered to become ‘new’ coastal lagoons or sea. Based on this criteria, the specified head and concentration boundary assigned to layer 1 for cases 1–5 are visualized in Fig. 6b,c,d.

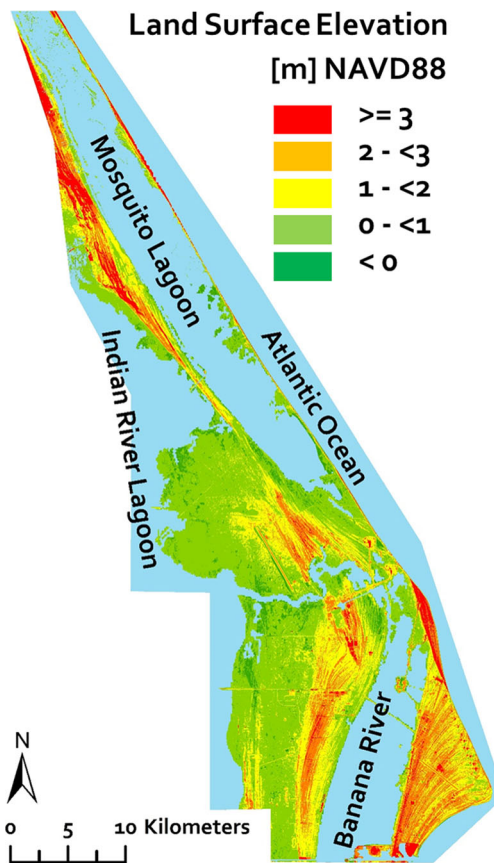


Fig. 5 Land surface elevation of the CCBIC. NAVD88 North American Vertical Datum of 1988

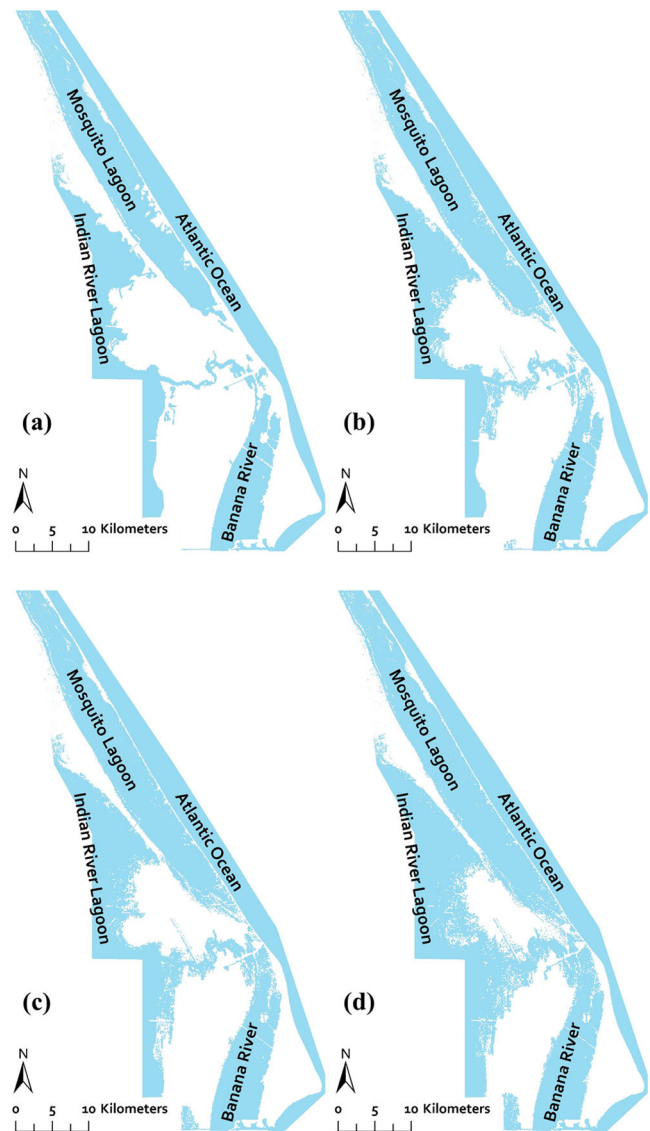


Fig. 6 Specified head and concentration boundary (marked in light blue) assigned to layer 1: **a** Case 0; **b** Cases 1 and 2; **c** Case 3; **d** Cases 4 and 5

Recharge boundary

The recharge boundary is assigned to represent the spatial variation of mean daily recharge from infiltrated rainwater. The mean daily recharge rate is estimated by mean daily precipitation measured from 2006 to 2014 given by the Tropical Rainfall Measuring Mission (TRMM) and recharge/precipitation (R/P) ratio mainly dependent on soil type and land use and land cover (Cherkauer and Ansari 2005; Dawes et al. 2012). The map of land use and land cover provided by the St. Johns River Water Management District (SJRWMD 2009) is shown in Fig. 7a. The R/P ratio is specified to 0 for urban areas and marshes/wetlands under the assumption that the land cover is comprised of impervious concrete for the former situation and the infiltration of rainwater is impeded by the saturated soil in the latter situation. The R/P ratios specified to forest, upland non-forest and cropland (agriculture) are 0.87, 0.96, and 0.87, respectively (Brauman et al. 2012). The spatial variation of mean daily recharge is visualized in Fig. 7b. The recharge rate is converted to zoned values and imported into the reference model in order to facilitate the calibration process. For the prediction/projection models, the recharge rate is assumed to increase/decrease proportionally with the increased/decreased precipitation; hence, the recharge rate is specified as a 17 % increase and 7 % decrease in cases 1 and 5 compared to case 0.

Evapotranspiration boundary

The evapotranspiration boundary is assigned to represent the spatial variation of mean daily evapotranspiration. In fact, the model input is mean daily potential evapotranspiration (PET) and vegetation extinction depth (ED), and mean daily evapotranspiration is computed by the SEAWAT code based on PET, ED, and simulated water-table depth. Mean daily PET (2006–2014) is given by the USGS Florida evapotranspiration network, and ED values are specified to 2.5, 1.45, and 2 m for forest, upland non-forest, and cropland, respectively (Shah et al. 2007).

Initial conditions

For steady-state models, it is not necessary to specify the starting water level and TDS concentration at each active model grid to be consistent with the designated aquifer properties and boundary conditions. In short, steady-state models do not require accurate starting heads and concentrations; however, reasonable estimates are required before start-up to avoid numerical instability. Thus, a steady-state one-layer SEAWAT model with a uniform grid spacing of 1,000 m in both the x- and y-directions

is implemented under 2010 hydrologic and hydrogeologic conditions in order to approximately estimate the water level and TDS concentration at each active model grid, and the output is the initial conditions for the reference model. Afterwards, the output of the calibrated reference model is the initial conditions for the five prediction/projection models.

Results and discussion

Present condition

Calibration

For the first-stage calibration, the hydraulic conductivity is adjusted using the trial-and-error method to minimize the differences between the simulated groundwater levels and the field-measured groundwater levels collected from 10 active observation wells (Fig. 8a). Daily groundwater levels monitored and recorded by each observation well during the period from 2006 to 2014 are averaged to represent the mean annual groundwater levels in 2010 as calibration targets. The calibration process does not terminate until the simulated groundwater levels match the observed groundwater levels to a satisfactory degree. Due to lack of observed groundwater levels from the central part of the CCBIC, the calibrated results might not accurately represent the true condition, and second-stage calibration is necessary.

For the second-stage calibration, the zoned recharge rate is adjusted using the trial-and-error approach to minimize the differences between the ‘simulated’ and ‘true’ wetlands. Due to the water table approaching the land surface (shallow water-table depth), wetlands are seasonally or permanently

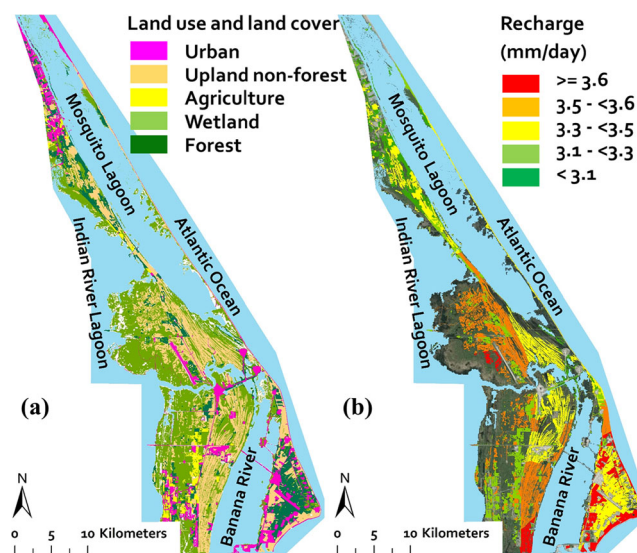


Fig. 7 a Land use and land cover; b Mean daily recharge (2010)

inundated. A uniform threshold of water-table depth cannot be defined because wetlands are highly complex ecological systems not only dependent on water-table depth. In order to perform the second-stage calibration, three conditions (conditions 1, 2 and 3) are proposed. For condition 1, the land areas where the simulated water-table depths are less than 0.2 m are speculated to be ‘simulated’ wetlands. In contrast, the land areas where the simulated water-table depths are greater than or equal to 0.2 m are deduced to be ‘simulated’ non-wetlands. Thereby, a map of ‘simulated’ wetlands and non-wetlands are plotted based on the model simulation results. For conditions 2 and 3, the thresholds of water-table depth are switched to 0.3 and 0.4 m, and two maps of ‘simulated’ wetlands and non-wetlands are plotted. The three maps are overlaid with the map of ‘true’ wetland, given by the land use and land cover map (Fig. 7a) produced by SJRWMD (2009). From the overlaid maps, some parts are ‘simulated’ wetlands and ‘true’ wetlands (situation A), and some parts are ‘simulated’ wetlands but not ‘true’ wetlands (situation B), and some parts are ‘simulated’ non-wetlands but ‘true’ wetlands (situation C), and some parts are ‘simulated’ non-wetlands and not ‘true’ wetlands (situation D). For each condition, the percentages of covering areas of situations A, B, C and D are computed, along with the percentage of consistency (the sum of percentages of covering areas of situations A and D because situations A and D indicate a consistency between the simulated results and the true conditions). A higher percentage of consistency is considered an indicator of better model performance.

After calibration, a Nash-Sutcliffe model efficiency coefficient (NSE) of 0.96 is achieved. From Table 3, the percentages of consistency are 64.6, 65.3, and 66.0 % for conditions 1, 2 and 3, respectively. The calibration results are considered acceptable. The horizontal and vertical hydraulic conductivity are calibrated to 360 and 36 m/day, and the annual recharge is calibrated to vary from 846 to 1,606 mm.

Table 4 Growth rate of ‘influenced’ areas

Case	‘Influenced’ area (km ²) ^a	Percentage (%)	Growth rate (%)
0	46	9.0	–
1	93	18.2	9.2
2	111	21.8	12.8
3	174	34.0	25
4	245	47.9	38.9
5	252	49.3	40.3
6	128	25.1	16.1
7	146	28.6	19.6
8	246	48.1	39.1
9	344	67.3	58.3
10	353	69.1	60.1

^a The total land area of the CCBIC was 511 km² in 2010

It should be noted that a good match between the simulated and observed groundwater levels is achieved. It is understandable that the simulated and observed groundwater levels from wells 2 and 4 are slightly different due to the boundary effects, since their locations are close to the border. However, the ‘simulated’ and ‘true’ wetlands do not match very well. The discrepancies in the second-stage calibration appear to be most likely due to the definition of ‘simulated’ wetlands. In fact, wetlands are complicated and dynamic natural systems composed of swamps, marshes, and bogs dependent not only on water-table depth but also topography, vegetation cover and soil type. However, the second-stage calibration is worthwhile although it is not optimal to determine wetlands only by simulated water-table depth. It is also expected that more observed data (especially groundwater salinity) will be available in the future for further model calibration.

Sensitivity analysis

Sensitivity analysis is carried out after model calibration. Sensitivity analysis is performed to explicitly determine the effects of small changes to model input on the simulated results by systematically modifying the input values within a reasonable range. The horizontal hydraulic conductivity (K_h) is model-wide varied and the zoned recharge rate (zones 1–10) is locally varied within a certain range. The sensitivity analysis results are shown in Fig. 8b. It can be observed that the simulated groundwater levels are most sensitive to changes in zones 7, moderately sensitive to changes in K_h and zones 2 and 8, and slightly sensitive to changes in zone 3. However, the results are insensitive to changes in zones 1, 4, 5, 6, 9 and 10. It is reasonable that the simulated groundwater levels are most sensitive to zone 7 in that this zone lies in east-central Merritt Island (Fig. 8a), which is comprised of high sand ridges serving as the primary recharge areas and the recharge rate specified to this zone determines how much freshwater is able to recharge the SAS.

However, it should be noted that the sensitivity analysis results might be biased because of the limitation of calibration targets. As mentioned earlier, the observation wells are not evenly distributed (located in the north and south Merritt Island) and no observation wells are in Cape Canaveral Island, which is partly the reason that the calibrated results are not sensitive to changes of recharge rate applied to Cape Canaveral Island.

Water-table depth

The simulated mean water-table depth in 2010 is visualized in Fig. 9a. In general, the water-table depth is shallow (less than 0.5 m) in west Merritt Island, but is deep (greater than 1 m) in the upland sand ridges in east Merritt Island, Cape Canaveral

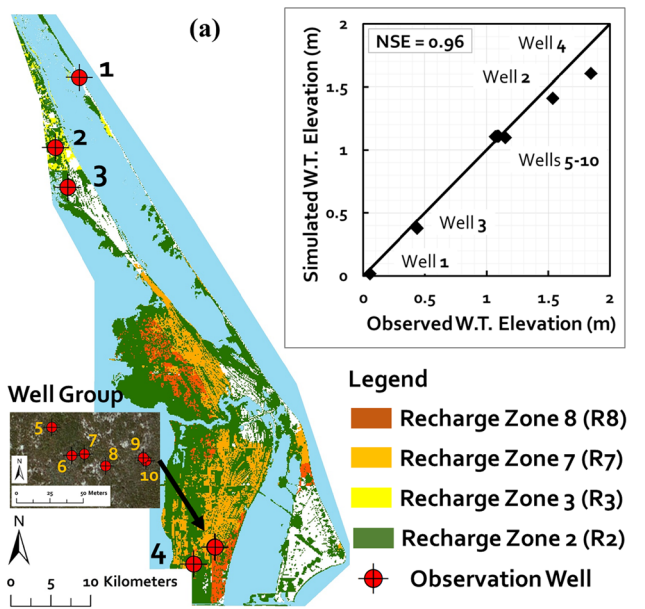


Fig. 8 **a** Location of observation wells and scatter diagram of the goodness of fit between the observed and simulated water-table elevations (*W.T.*, m NAVD88); *NSE* Nash-Sutcliffe model efficiency coefficient. **b** Sensitivity of horizontal hydraulic conductivity (K_i) and recharge

Island, and the northwestern coastal highlands. A positive water-table depth indicates that the water table is below land surface, while a negative value represents the opposite condition. It is postulated that the areas with negative values have a high risk of being frequently or permanently inundated due to the water table approaching or breaching land surface, and are referred to as ‘sensitive’ areas. These ‘sensitive’ areas are highlighted in yellow-brown in Fig. 9b. Based on the simulated results, it is estimated that the ‘sensitive’ areas account for 21.7 % of the total land area in 2010.

Salinity

According to NGWA (2010), the TDS concentration of the saltwater/freshwater transition zone is between 1,000 and 35,000 mg/L, which is higher than freshwater (less than

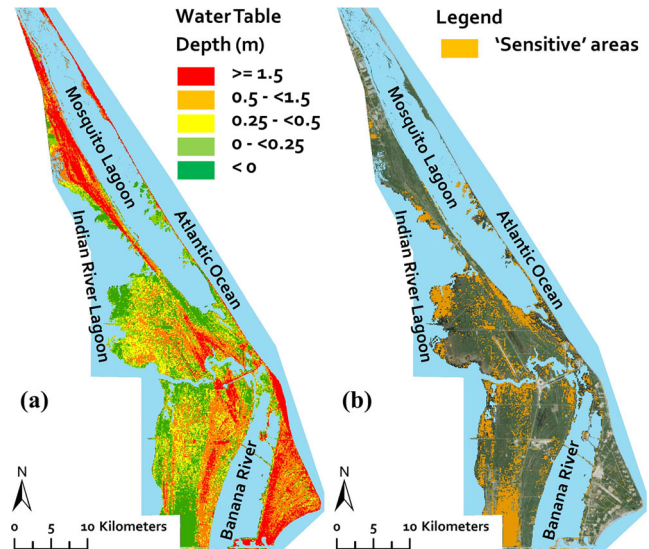


Fig. 9 Spatial variation of: **a** Water-table depth; **b** ‘Sensitive’ areas

1,000 mg/L) and lower than seawater (35,000 mg/L), and the water quality is defined as slightly saline water (1,000–3,000 mg/L), moderately saline water (3,000–10,000 mg/L), and highly saline water (10,000–35,000 mg/L). The plan view of the transition zone is shown in Fig. 10a. The simulated values of TDS concentrations are extracted from model layer 3 (the model consists of five layers and layer 3 is the middle layer). In general, the transition zone covers a larger area in west Merritt Island where the saltwater wedge toe even trespasses 3–4 km inland, indicating a greater groundwater salinity than other locations. The areas that TDS concentrations are greater than freshwater are referred to as ‘influenced’ areas shown in Fig. 10a. It is estimated that the ‘influenced’ areas account for 9 % of the total land area in 2010. The vertical view of the transition zone is shown in Fig. 10b (the west to east cross-section labeled A–A’ in Fig. 10b). The widths of the zones of slightly saline water and moderately saline water are approximately 0.5 km, and the width of the zone of highly saline water is approximately 3 km.

Discussion

The vertical view of land surface and water-table elevation on Merritt Island is shown in Fig. 10c (the west to east cross-section labeled 1–1’ in Fig. 10a). In most places in west Merritt Island, land surface is low and water-table depth is shallow. A heavy rainfall event might cause a rapid rising of the water table above land surface resulting in overland flooding; besides, the marshes/wetlands located there are highly vulnerable to wind-driven coastal flooding induced by storm surge and hurricanes. In addition, freshwater recharge is impeded because of the shallow water-table depth; thus, groundwater salinity in west Merritt Island is higher than

other places. In Cape Canaveral Island and east Merritt Island, land surface is higher and water-table depth is deeper compared to west Merritt Island. Additionally, freshwater recharge is higher because of the high permeability of sand; therefore, fewer areas are vulnerable to overland flooding, and ground-water salinity is lower.

It should be noted that the spatial distribution of ‘sensitive’ areas and ‘influenced’ areas might expand and shrink with the annual cycles of sea level and rainfall; however, the dynamic expansion and shrinkage are not simulated, since the reference model assumes a steady-state condition. Future research may be able to quantify the dynamic changes of the ‘sensitive’ areas by changing the temporal scale from yearly to monthly and developing a transient model.

Climate change impacts

Based on the calibrated reference model, five prediction/projection models are developed by modification of the specified head and concentration boundary and the recharge boundary to represent SLR and precipitation change while keeping other boundary conditions unchanged from 2010.

Effect of SLR

Cases 2, 3, and 4 represent 13.2, 31.0, and 58.5 cm SLR (refer to Table 1), and the predicted ‘sensitive’ areas are highlighted in yellow-brown in Fig. 11c,d,e, respectively. The simulated ‘sensitive’ areas of case 0 are also shown in Fig. 11a for

reference. Compared to case 0, the ‘sensitive’ areas of cases 2, 3 and 4 account for 26.6, 36.0, and 47.2 % of the total land area, with a growth rate of 4.9, 14.3 and 25.5 %. The predicted ‘sensitive’ areas are mainly found in west Merritt Island, and expand corresponding to SLR. The predicted ‘influenced’ areas are shown in Fig. 12c,d,e, respectively. The predicted salinity is extracted from model layer 3. The simulated ‘influenced’ areas of case 0 are also shown in Fig. 12a for reference. Compared to case 0, the ‘influenced’ areas of cases 2, 3 and 4 account for 21.8, 34, and 47.9 % of the total land area, with a growth rate of 12.8, 25, and 38.9 %, respectively. The landward migration of saline water mostly occurs in west Merritt Island, and the saltwater wedge toe trespasses 8–10 km inland in some locations, indicating the occurrence of SLR-induced SWI. However, it seems that the effect of SLR on Cape Canaveral Island is not significant.

Coupled effects of SLR and precipitation change

Case 1 represents 13.2 cm SLR coupled with a 17 % increase in precipitation, and case 5 represents 58.5 cm SLR coupled with a 7 % decrease in precipitation (refer to Table 1). In order to quantify the effect of precipitation change, case 1 results are compared to case 2, and case 5 results are compared to case 4, since the SLR scenarios of cases 1 and 2, along with cases 4 and 5, are the same.

The predicted ‘sensitive’ areas of cases 1 and 5 are highlighted in yellow-brown in Fig. 11b,f. For case 1, the ‘sensitive’ areas account for 32.1 % of the total land area,

Fig. 10 Spatial variation of: **a** ‘Influenced’ areas (plan view); **b** ‘Influenced’ areas (west to east cross-section labeled A–A’); **c** Elevation of land surface and water table (west to east cross-section labeled I–I’)

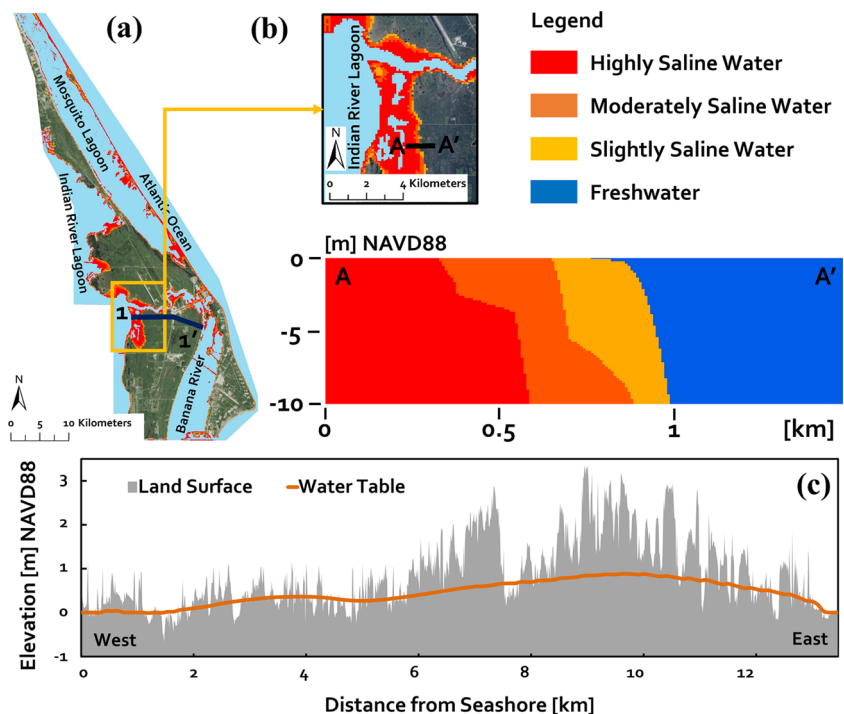
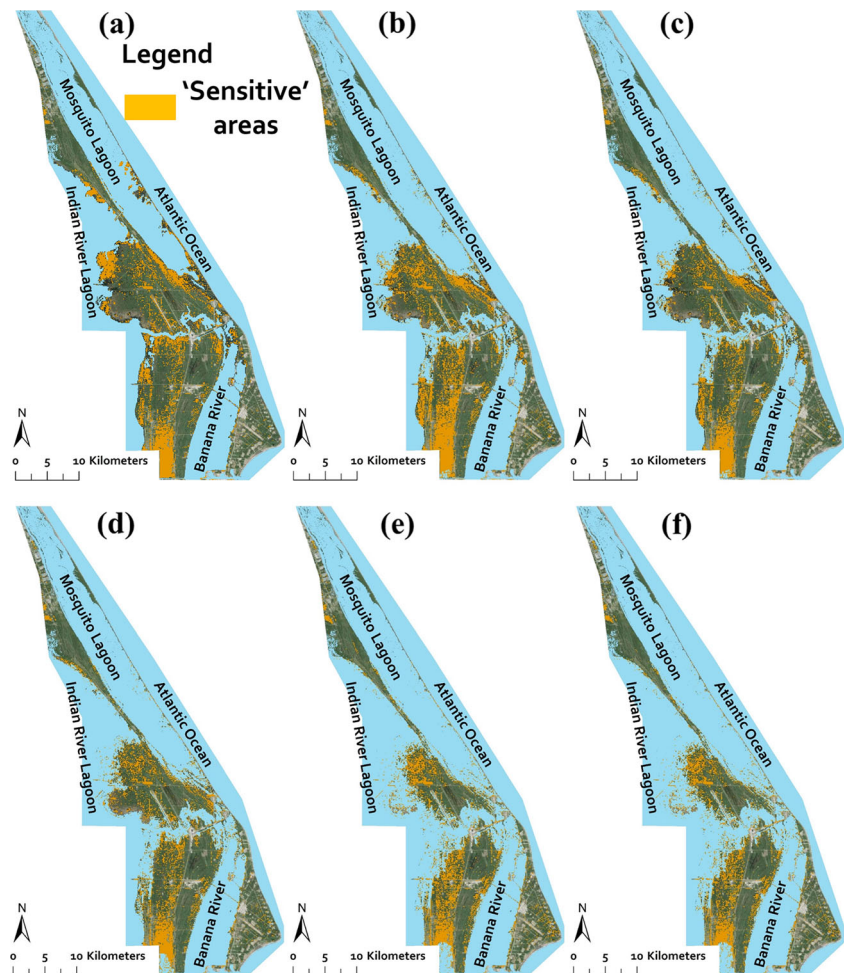


Fig. 11 Spatial variation of ‘sensitive’ areas: **a** Case 0; **b** Case 1 (13.2 cm SLR, +17 % precipitation); **c** Case 2 (13.2 cm SLR); **d** Case 3 (31.0 cm SLR); **e** Case 4 (58.5 cm SLR); **f** Case 5 (58.5 cm SLR, -7 % precipitation)



compared to case 0 (21.7 %) and case 2 (26.6 %). For case 5, the ‘sensitive’ areas account for 45.8 % of the total land area, compared to case 4 (47.2 %). The predicted ‘influenced’ areas of cases 1 and 5 are shown in Fig. 12b,f. For case 1, the ‘influenced’ areas account for 18.2 % of the total land area, compared to case 0 (9 %) and case 2 (21.8 %). For case 5, the ‘influenced’ areas account for 49.3 % of the total land area, compared to case 4 (47.9 %). Similarly, the ‘sensitive’ and ‘influenced’ areas are mainly found in west Merritt Island, and the coupled effects are not significant on Cape Canaveral Island.

Discussion

The predicted results indicate that the effects of SLR and precipitation change are significant for west Merritt Island. This area is particularly vulnerable because of its low-lying coastal areas with flat topography and shallow water-table depth, indicating a high risk of being inundated during and after an extreme rainfall event. Also, low land-surface elevation corresponding with low potential for freshwater recharge due to a shallow water table, results in a low fresh-groundwater-pressure head and low hydraulic-head gradient between inland

fresh groundwater and coastal saline groundwater, which further results in a low rate of submarine groundwater discharge, which reduces the protection from SLR-induced SWI offered by freshwater groundwater recharge. In west Merritt Island, the land cover is mainly composed of fresh marsh, intermediate marsh (less saline than brackish), brackish marsh, and saline marsh. Landward migration of saline water into the traditionally freshwater areas can cause degradation of the ecologic system and alter the distribution and productivity of vegetation communities. Increased rainfall can contribute to flushing, while a prolonged drought can intensify salinity problems. Salt tolerance of plant communities is dependent on vegetation type, duration of exposure to saline water, rate of salinity increase, mineral content of soil, and degree of submergence (Webb and Mendelssohn 1996; Howard and Mendelssohn 1999). Some species can tolerate a wide range of salinity, and can recover quickly once the salinity declines; however, some species die off quickly and cannot recover. Potential consequences of exposure to salinity include, but are not limited to, shift of wetland from fresh or less saline marsh to brackish or saline marsh, vegetation species dieback and limited recovery, shift in vegetation species composition from less salinity-tolerant species to more salinity-tolerant

species, and reduction in biomass production (Steyer et al. 2007). SWI not only affects marshes/wetlands, but also affects agriculture as well. Citrus is the main agricultural product in this area, and a reduction in citrus production due to increased groundwater salinity might be a big problem. Currently, no pumping wells are designed for human consumption in this area, and SWI does not have a negative effect on the public drinking-water supply.

The predicted results indicate that the effects of SLR and precipitation change are not significant on Cape Canaveral Island and east Merritt Island. This area serves as the primary recharge area due to its high elevation, deep water-table depth, land cover (forest and pasture) and soil type (sand). Because of the highly permeable sand, infiltration of rainwater is facilitated, which generates a high freshwater pressure head, resulting in a high rate of submarine groundwater discharge from inland fresh groundwater zone to coastal saline groundwater zone. This builds up an effective freshwater hydraulic barrier to prevent the landward migration of saline groundwater and alleviate the negative effects of SWI to some extent; however, it is estimated that the negative effects could be noticeable if SLR and precipitation change turn out to be greater than projected.

Five additional cases (cases 6–10) are simulated for further investigation of the effects of SLR and precipitation change on SWI, the key factors that determine whether SWI occurs and how far inland the saltwater wedge toe invades. Cases 7, 8 and 9 quantify the effect of 23.4, 59, and 119.5 cm SLR. Case 6 quantifies the coupled effects of 23.4 cm SLR and +16 % precipitation, while case 10 quantifies the coupled effects of 119.5 cm SLR and –11 % precipitation. These scenarios are the estimated projections for 2080 (Rosenzweig et al. 2014). The growth rate of the ‘influenced’ areas where SWI occur are computed and described in Table 4 and plotted in Fig. 13a. In order to differentiate the effect of SLR and precipitation change, the growth rate of cases 2, 3, 4, 7, 8 and 9 are plotted as red circles and the growth rate of cases 1, 5, 6 and 10 are plotted as yellow-brown triangles. An interpolation of the growth rate based on cases 2, 3, 4, 7, 8 and 9 (red circles) is also plotted.

In Fig. 13a, the growth rate increases faster at first and then slightly declines. At the beginning, the growth rate increases sharply in that west Merritt Island is vulnerable to SLR even though the amount is small due to its low elevation and flat topography. Afterwards, the growth rate slightly declines because the amount of SLR is not large enough to affect Cape Canaveral Island and east Merritt Island significantly. Using the SLR scenarios applied in this study, the growth rate of the ‘influenced’ areas under other potential SLR scenarios can be roughly estimated by the interpolation as shown in Fig. 13a. For example, the growth rate might increase to 35 and 52 % when SLR is 50 and 100 cm, indicating potential ‘influenced’ areas of 225 and 312 km², respectively. The growth rate is also

altered by increased/decreased precipitation. Compared to case 2, +17 % precipitation (case 1) generates a growth rate of –3.52 %; compared to case 4, –7 % precipitation (case 5) generates a growth rate of 1.37 %; compared to case 7, +16 % precipitation (case 6) generates a growth rate of –3.52 %; Compared to cases 9, –11 % precipitation (case 10) generates a growth rate of 1.76 %. The relationship between increased/decreased precipitation and its impacts on alteration of growth rate is plotted in Fig. 13b. According to linear interpolation, in order to offset the effect of SLR for cases 2, 3 and 4, an increased precipitation of 63.0, 125.6 and 195.4 % is required. This estimate is based on the assumption that recharge increases/decreases proportionally with precipitation. In fact, an increased recharge of 63.0, 125.6 and 195.4 % is required.

In order to prevent SWI, it is of great importance to minimize the effect of SLR, since its effect is clearly more influential than the effect of precipitation change. In order to ‘balance’ SLR, it is necessary to increase the inland fresh groundwater pressure head by artificial recharge. Recharge wells could be constructed close to the coastline, along with detention ponds designed for flood control to avoid inland flooding, since the CCBIC is humid subtropical with plenty of precipitation especially in the rainy season. The designed detention ponds could be used to temporarily hold the excess rainwater while slowly draining to the coastal recharge wells. Artificial recharge is even more important in the dry season because of less precipitation. It is not necessary to shut down the two pumping wells, which are used occasionally for lawn irrigation, since the pumping rates are very low and the effect is tiny.

It should be noted that the results might be biased due to the following reasons. Firstly, the calibration targets are limited due to a lack of observation wells, resulting in a less robust model calibration. It is expected that more observed groundwater level and salinity data would be available for future model calibration. Secondly, the effect of heterogeneity on the spatial variation of water-table depth and groundwater salinity is not considered. Due to lack of geophysical surveys and borehole tests, the spatial variation of hydraulic conductivity is unavailable, and the SAS is assumed to be homogeneous with a uniform value assigned initially to all model grids expected to be adjusted during calibration. Thirdly, the effects of different water levels and TDS concentrations in the coastal lagoons and the Atlantic Ocean are not considered. The mean water levels of the coastal lagoons are usually slightly higher than the Atlantic Ocean (10 cm approximately). The TDS concentrations of the coastal lagoons and the Atlantic Ocean are varied spatially, affected by climate factors and human activities. In some locations, the TDS concentrations of the coastal lagoons are higher than 35,000 mg/L, particularly during the dry season because of large amounts of water loss due to evaporation and drainage. The TDS concentrations of the nearshore Atlantic Ocean might be lower than 35,000 mg/L

Fig. 12 Spatial variation of ‘influenced’ areas: **a** Case 0; **b** Case 1 (13.2 cm SLR, +17 % precipitation); **c** Case 2 (13.2 cm SLR); **d** Case 3 (31.0 cm SLR); **e** Case 4 (58.5 cm SLR); **f** Case 5 (58.5 cm SLR, -7 % precipitation)

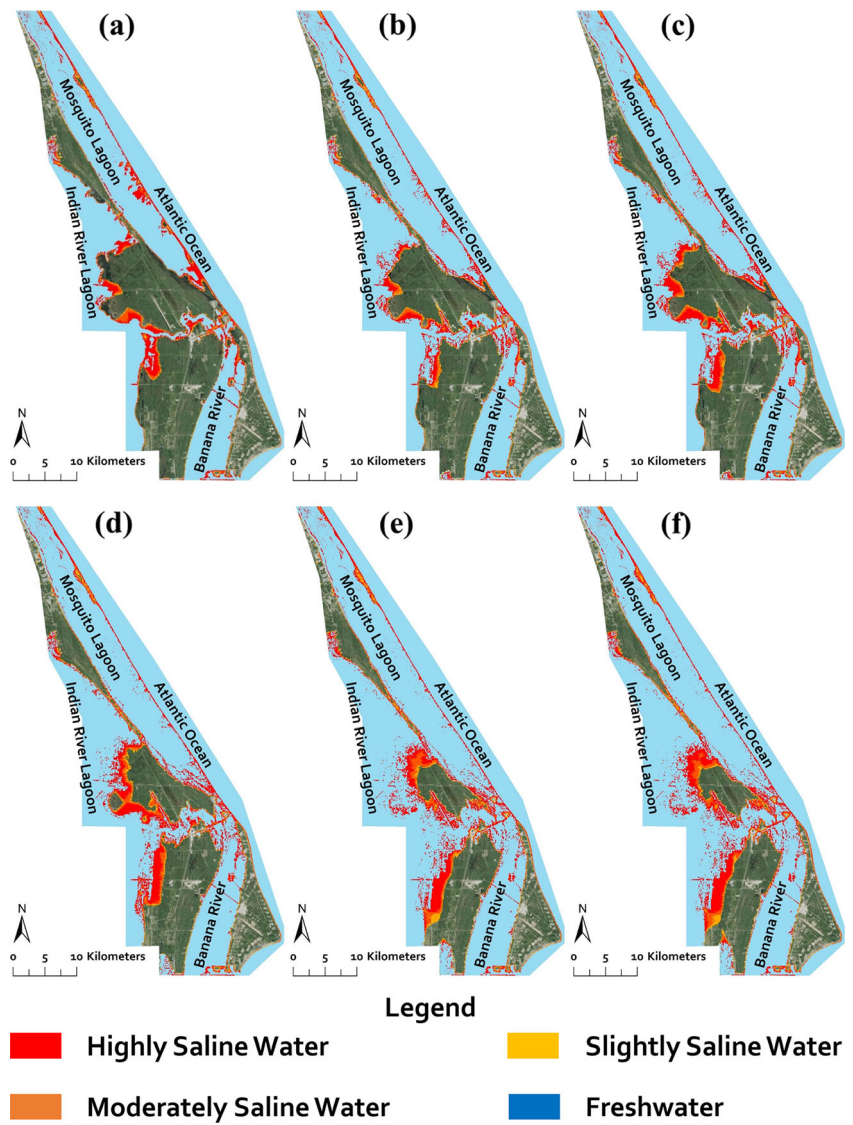
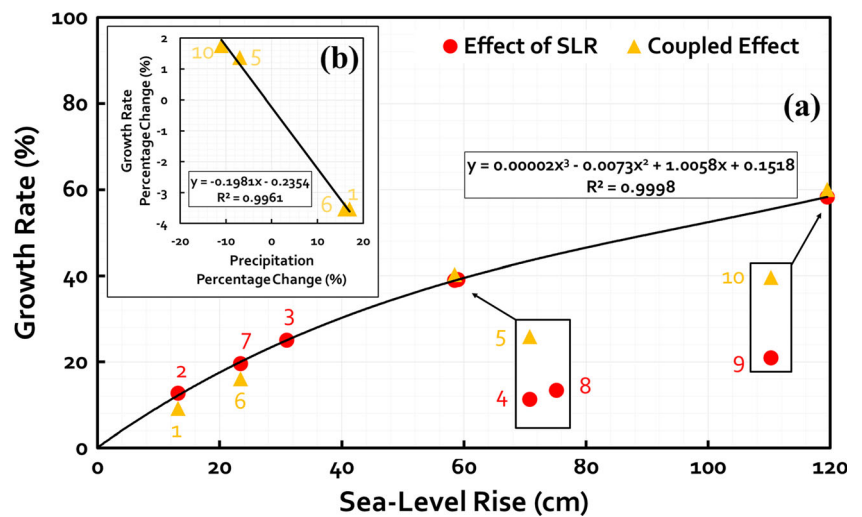


Fig. 13 a Growth rate of ‘influenced’ areas; **b** The relationship between increased/decreased precipitation and its impacts on alteration of growth rate



because of submarine groundwater discharge. However, due to lack of the relevant recorded water levels and TDS concentrations, water levels of the coastal lagoons are assumed to be exactly the same with the Atlantic Ocean, and TDS concentrations of the coastal lagoons and the Atlantic Ocean are assumed to be equal to 35,000 mg/L. Fourthly, upward migration of saline water from the underlying highly-mineralized FAS is not simulated. The situation of SWI might be even worse than predicted if the upward groundwater seepage from the FAS is considered. Fifth, the ‘new’ coastline determined for the predicted models under various SLR scenarios contain high levels of uncertainty, resulting in the predicted results probably being over- or under-estimated. Based on the preceding explanations, the results might be biased and the discrepancies are probably due to the simplification of the model implementation. Future research will take other climate change factors into consideration, including increasing the number and size of extreme weather events such as hurricane and storm surge, and higher mean annual temperature and potential evaporation.

Conclusions

The purpose of this study is to quantitatively evaluate the impacts of climate change on water-table depth and salinity distribution in the shallow unconfined coastal aquifer of alluvial shorelines and barrier island systems. The selected study site is the CCBIC region in east-central Florida, where the associated Kennedy Space Center, Cape Canaveral Air Force Station, Merritt Island National Wildlife Refuge and Canaveral National Sea Shore are located. Numerical models using the SEAWAT code are implemented and parameterized with the relevant regional geologic, hydrogeologic and hydrologic features in order to achieve this goal.

The reference model is calibrated against monitored heads and saltwater/freshwater marsh/wetland categorized in the land use and land cover map. Reasonable agreements between the simulated results and field-measured data are achieved, indicating that the simulation results are representative of 2010 hydrogeologic conditions. Further calibration is required for future model updates when sufficient field-measured TDS concentrations become available. Results indicate that climate change in the form of precipitation change and SLR, play an undeniable role in altering the water-table depth and water quality in the surficial aquifer within the CCBIC region. The simulated salinity migration and fluctuation of water-table depth can contribute to ongoing attempts at forecasting vegetation community responses to these climate change related variables. Moreover, the developed SEAWAT models can be utilized as an effective tool for coastal water-resources management, land use planning, and adaptation decision-making in a changing climate.

Acknowledgements This research was funded in part by the NASA Kennedy Space Center, Ecological Program, Climate Adaptation Science Investigators (CASI) project (Award: IHA-SA-13-006) and the Louisiana Sea Grant Laborde Chair Endowment.

References

- Anderson MP, Woessner WW (1991) Applied groundwater modeling: simulation of flow and advective transport. Academic, San Diego
- Barlow PM, Reichard EG (2010) Saltwater intrusion in coastal regions of North America. *Hydrogeology J* 18:247–260
- Bear J (1979) *Hydraulics of groundwater*. McGraw-Hill, New York
- Bear J, Cheng A, Sorek S, Ouazar D, Herrera I (1999) *Seawater Intrusion in coastal aquifers: concepts, methods and practices (theory and applications of transport in porous media)*. Kluwer, Dordrecht, The Netherlands
- Bilskie MV, Hagen SC, Medeiros SC, Passeri DL (2014) Dynamics of sea level rise and coastal flooding on a changing landscape. *Geophys Res Lett* 41(3):927–934
- Blandford TN, Birdie T, Robertson JB (1991) Regional groundwater flow modeling for East-Central Florida with emphasis on eastern and central Orange County. St. Johns River Water Management District Special Publication SJ91-SP4, St. Johns River Water Management, Palatka, FL
- Brauman KA, Freyberg DL, Daily GC (2012) Land cover effects on groundwater recharge in the tropics: ecohydrologic mechanisms. *Ecohydrology* 5:435–444
- Chang SW, Clement TP, Simpson MJ, Lee K (2011) Does sea-level rise have an impact on saltwater intrusion? *Adv Water Resour* 34:1283–1291
- Cherkauer DS, Ansari SA (2005) Estimating ground water recharge from topography, hydrogeology, and land cover. *Groundwater* 43(1):102–112
- Cobaner M, Yurtal R, Dogan A, Motz LH (2012) Three-dimensional simulation of seawater intrusion in coastal aquifers: a case study in the Goksu Deltaic Plain. *J Hydrol* 464–465:262–280
- Dausman AM, Langevin CD, Bakker M, Schaars F (2010) A comparison between SWI and SEAWAT: the importance of dispersion, inversion and vertical anisotropy. 21st Saltwater Intrusion Meeting, Azores, Portugal, June 2010. http://www.swim-site.nl/pdf/swim21/pages_271_274.pdf. Accessed 11 May 2016
- Dawes W, Ali R, Varma S, Emelyanova I, Hodgson G, McFarlane D (2012) Modelling the effects of climate and land cover change on groundwater recharge in south-west Western Australia. *Hydrol Earth Syst Sci* 16:2709–2722
- Freeze RA, Cherry JA (1979) *Groundwater*. Prentice Hall, Englewood Cliffs, NJ
- Guo W, Langevin CD (2002) User’s guide to SEAWAT: a computer program for simulation of three-dimensional variable-density ground-water flow. *Techniques of Water-Resour Invest*, Book 6, USGS, Reston, VA
- Hall CR, Schmalzer PA, Breininger DR, Duncan BW, Drese JH, Scheidt DA, Lowers RH, Reyier EA, Holloway-Adkins KG, Oddy DM, Cancro NR, Provancha JA, Foster TE, Stolen ED (2014) Ecological impacts of the space Shuttle Program at John F. Kennedy Space Center, Florida. NASA/TM-2014-216639, NASA, Washington, DC
- Howard RJ, Mendelsohn IA (1999) Salinity as a constraint on growth of oligohaline marsh macrophytes: I. species variation in stress tolerance. *Am J Bot* 86(6):785–794
- Hutchings WC, Tarbox DL, and HSA engineers and scientists (2003) A model of seawater intrusion in surficial and confined aquifers of northeast Florida. The 2nd International Conference on Saltwater Intrusion and Coastal Aquifers: Monitoring, Modeling, and

- Management. http://www.olemiss.edu/sciencenet/saltnet/swica2/Hutchings_ext.pdf. Accessed 2 May 2016
- Langevin CD (2003) Simulation of submarine groundwater discharge to a marine estuary: Biscayne Bay, Florida. *Groundwater* 41(6):758–771
- Langevin CD, Thorne DT, Dausman AM, Sukop MC, Guo W (2008) SEAWAT Version 4: a computer program for simulation of multi-species solute and heat transport. US Geological Survey Techniques and Methods, Book 6, USGS, Reston, VA
- Lin J, Snodsmith B, Zheng C, Wu J (2009) A modeling study of seawater intrusion in Alabama Gulf Coast, USA. *Environ Geol* 57:119–130
- Mailander JL (1990) Climate of the Kennedy Space Center and vicinity. NASA Tech. Memo. 103498, NASA, Washington, DC
- Masterson JP, Fienen MN, Thieler ER, Gesch DB, Gutierrez BT, Plant NG (2014) Effects of sea-level rise on barrier island groundwater system dynamics: ecohydrological implications. *Ecohydrology* 7:1064–1071
- McGurk B, Presley PF (2002) Simulation of the effects of groundwater withdrawals on the Floridan Aquifer System in East-Central Florida: model expansion and revision. St. Johns River Water Management District Technical Publication, SJ2002-5, St. Johns River Water Management, Palatka, FL
- Nakada S, Yasumoto J, Taniguchi M, Ishitobi T (2011) Submarine groundwater discharge and seawater circulation in a subterranean estuary beneath a tidal flat. *Hydrol Process* 25:2755–2763
- NGWA (2010) Brackish groundwater. National Groundwater Association Information Brief. http://www.ngwa.org/media-center/briefs/documents/brackish_water_info_brief_2010.pdf. Accessed June 2016
- Nicholls RJ, Cazenave A (2010) Sea-level rise and its impact on coastal zones. *Science* 328(18):1517–1520
- Oude Essink GHP, Van Baaren ES, De Louw PGB (2010) Effects of climate change on coastal groundwater systems: a modeling study in the Netherlands. *Water Resour Res*. doi:10.1029/2009WR008719
- Parker BB (1991) Sea level as an indicator of climate and global change. *Mar Technol Soc J* 25(4):13–24
- Passeri DL, Hagen SC, Medeiros SC, Bilskie MV, Alizad K, Wang D (2015) The dynamic effects of sea level rise on low-gradient coastal landscapes: a review. *Earth's Future* 3(6):159–181
- Qahman K, Larabi A (2006) Evaluation and numerical modeling of seawater intrusion in the Gaza aquifer (Palestine). *Hydrogeol J* 14:713–728
- Rasmussen P, Sonnenborg TO, Gonciar G, Hinsby K (2013) Assessing impacts of climate change, sea level rise, and drainage canals on saltwater intrusion on coastal aquifer. *Hydrol Earth Syst Sci* 17:421–443
- Rosenzweig C, Horton RM, Bader DA, Brown ME, DeYoung R, Dominguez O, Fellows M, Friedl L, Graham W, Hall C, Higuchi S, Iraci L, Jedlovec G, Kaye J, Loewenstein M, Mace T, Milesi C, Patzert W, Stackhouse PW, Touffectis K (2014) Enhancing climate resilience at NASA centers: a collaboration between science and stewardship. *Bull Am Meteorol Soc* 95(9):1351–1363
- Sanford WE, Pope JP (2010) Current challenges using models to forecast seawater intrusion: lessons from the Eastern Shore of Virginia, USA. *Hydrogeology J* 18:73–93
- Scanlon BR, Mace RE, Barrett ME, Smith B (2003) Can we simulate regional groundwater flow in a karst system using equivalent porous media models? Case study, Barton Springs Edwards aquifer, USA. *J Hydrol* 276:137–158
- Schmalzer PA, Hinkle GR (1990) Geology, geohydrology and soils of Kennedy Space Center: a review. NASA Tech. Memo. 103813, NASA, Washington, DC. <http://ntrs.nasa.gov/archive/nasa/casi.ntrs.nasa.gov/19910001129.pdf>. Accessed 2 May 2016
- Schmalzer PA, Hensley MA, Mota M, Hall CR, Dunlevy CA (2000) Soil, groundwater, surface water, and sediments of Kennedy Space Center, Florida: background chemical and physical characteristics. NASA/Technical Memorandum-2000-208583, NASA, <http://ntrs.nasa.gov/archive/nasa/casi.ntrs.nasa.gov/20000116077.pdf>. Accessed 1 May 2016
- Shah N, Nachabe M, Ross M (2007) Extinction depth and evapotranspiration from ground water under selected land covers. *Groundwater* 45(3):329–338
- Sharqawy MH, Lienhard JH, Zubair SM (2010) Thermophysical properties of seawater: a review of existing correlations and data. *Desalin Water Treat* 16:354–380
- Sherif MM, Singh VP (1999) Effect of climate change on sea water intrusion in coastal aquifers. *Hydrol Process* 13:1277–1287
- Shoemaker WB, Edwards KM (2003) Potential for saltwater intrusion into the Lower Tamiami Aquifer near Bonita Springs, southwestern Florida. US Geol Surv Water Resour Invest Rep 03-4262
- SJRWMD (2009) Land cover/land use. St. Johns River Water Management District GIS data. SJRWMD, Palatka, FL. <http://www.sjrwmd.com/gisdevelopment/docs/themes.html>. Accessed June 2016
- Steyer GD, Perez BC, Piazza S, Suir G (2007) Potential consequences of saltwater intrusion associated with hurricanes Katrina and Rita. In: Farris GS, Smith GJ, Crane MP, Demas CR, Robbins LL, Lavoie DL (eds) Science and the storms: the USGS responses to the hurricanes of 2005. US Geological Survey, Reston, VA
- Sulzbacher H, Wiederhold H, Siemon B, Grinat M, Igel J, Burschil T, Günther T, Hinsby K (2012) Numerical modelling of climate change impacts on freshwater lenses on the North Sea Island of Borkum using hydrological and geophysical methods. *Hydrol Earth Syst Sci* 16:3621–3643
- Tang Y, Tang Q, Tian F, Zhang Z, Liu G (2013) Responses of natural runoff to recent climatic variations in the Yellow River basin, China. *Hydrol Earth Syst Sci* 17:4471–4480
- Webb MD, Howard KWF (2011) Modeling the transient response of saline intrusion to rising sea-levels. *Groundwater* 49(4):560–569
- Webb EC, Mendelssohn IA (1996) Factors affecting vegetation dieback of an oligohaline marsh in coastal Louisiana: field manipulation of salinity and submergence. *Am J Bot* 83(11):1429–1434
- Werner AD, Simmons CT (2009) Impact of sea-level rise on sea water intrusion in coastal aquifers. *Groundwater* 47(2):197–204
- Werner AD, Bakker M, Post VEA, Vandenbohede A, Lu C, Ataie-Ashtiani B, Simmons CT, Barry DA (2013) Seawater intrusion processes, investigation and management: recent advances and future challenges. *Adv Water Resour* 51:3–26